Table IV. Comparison of imaging modalities for the identification of the primary lesion in patients with bone metastasis.

A, Time interval for detection of the primary lesion with different imaging modalities

Imaging modality	Detection of primary lesion/total number of patients	Interval between first visit and examination (days)
CT scan	32/55	3.6
PET-CT	17/39	7.2
Bone scan	0/43	6.3
Tl scan	0/13	5.5

B, Number of cases with different primary lesions detected with CT or PET-CT

	Method of identification of primary lesion			
Primary lesion	CT	PET	CT alone	PET alone
Lung	16	6	0	1
Kidney	3	1	0	0
Thyroid	2	0	1	0
Bladder	2	0	2	0
Pancreas	2	0	0	0
Myeloma	2	1	2	1
Gastric	1	1	0	0
Liver	1	1	0	0
Colorectal	1	2	0	1
Lymphoma	1	0	0	0
GIST	1	0	0	0
Prostate	0	4	0	0
Breast	0	1	0	0
Total	32	17	5	3

PET-CT, positron emission tomography-computed tomography.

all patients with bone metastasis. Our results indicated a relatively good prognosis compared to those of a previous study (12). In addition, the survival rates were significantly lower in patients in the non-spinal compared with those in the spinal metastatic group, which included all the patients with bone metastasis. Furthermore, our findings revealed that the number of breast cancer patients was higher in the spinal compared to that in the non-spinal metastatic group. Survival was significantly increased in breast cancer patients with bone metastasis compared to those with other primary lesions with bone metastasis (data not shown). These findings suggest that differences in the origin of the cancer may affect prognosis, depending on whether bone metastasis occurs in the spine or elsewhere.

We demonstrated that SREs exert a significant negative effect on survival. Although neurological complications did not appear to exert a statistically significant effect on survival in patients with spinal metastasis, the number of patients with neurological complications was statistically different between the PS≤1 and PS≥2 groups. These findings suggest that the incidence of neurological complications was increased in the group with PS≥2 and negatively affected survival. In addition, Katagiri *et al* (11) reported that PS scores of 3 or 4 were a significant poor prognostic factor. Our findings suggest that a PS score of 2 may also exert a negative effect on prognosis in patients with bone metastasis.

We observed that the primary lesion distribution differed depending on whether the primary tumor was known or unknown at the initial visit. In the primary-known group, the most frequent primary cancer was breast cancer, followed by lung, liver and thyroid cancer. Our findings suggest the significance of the follow-up of cancer patients with bone metastasis. In the primary-unknown group, the most frequent primary cancer was lung cancer, followed by myeloma, kidney and prostate cancer. Consistent with our results, Iizuka *et al* (4) reported that myeloma was the most common primary malignancy in cases with spinal metastasis of unknown origin, followed by lung and prostate cancer. Destombe *et al* (3) reported that the most frequent primary cancer was lung, followed by breast cancer. These findings suggest that, when evaluating bone metastatic patients with unknown primary tumors, clinical examinations should be performed taking into consideration the possibility of diagnosing these primary cancers. During the follow-up period, the primary lesion was not identified in 5 cases. It was reported that lung and pancreatic cancer were the most frequent primary lesions in autopsy studies (13,14). Our findings demonstrated that pancreatic cancer was diagnosed as the primary lesion in only 2 cases (3%) in the primary-unknown group. These findings suggest that more detailed examinations, including magnetic resonance cholangiopancreatography or endoscopic retrograde cholangiopancreatography, may be required for bone metastatic patients in whom the primary lesion was not identified.

Although biopsy of the most accessible osseous lesion was routine during the examination, the proportion of an accurate final diagnosis in solid and hematopoietic tumors was low (4,5,15). In addition, biopsy requires invasive procedures. ^{18}F-FDG PET-CT whole-body imaging is non-invasive and highly sensitive. It has been reported that ^{18}F-FDG PET-CT should be used as a first-line imaging examination for patients with a primary carcinoma of unknown origin, rather than after other diagnostic procedures have failed to identify the primary lesion (16). Although ^{18}F-FDG PET-CT is useful in helping physicians locate the primary lesion, patients were required to wait an average of 7.2 days for an ^{18}F-FDG PET-CT examination, due to the long waiting list. We demonstrated that CT scans helped identify 32 of the 55 (58%) primary lesions within 3.6 days from the time of the patient's first visit. Therefore, a CT scan is a rapid examination, valuable for the identification of the primary lesion of a bone metastasis. In addition, we did not observe a statistically significant difference in utility between CT and ^{18}F-FDG PET-CT in establishing the origin of a bone metastasis. Our findings suggest that a CT scan should be performed prior to an ^{18}F-FDG PET-CT scan, particularly if the latter requires a waiting period of several days.

To improve the prognosis of patients with metastatic bone tumors, a team approach is required, comprising an orthopaedic surgeon along with a specialist to manage

treatment of the primary tumor, a radiologist, rehabilitation staff and a palliative care team (17). Collaboration is essential to developing a treatment strategy that may be tailored to the individual patient (18). In this regard, our department has established a bone metastasis registration system that encompasses all specialties in our hospital and is accessible to each specialty.

In conclusion, our findings demonstrated that several factors may be related to patient prognosis and the effectiveness of CT; these factors may prove useful in determining the origin of the primary lesion. Further examination of prognostic factors and advancements in diagnostic imaging may improve the treatment of patients with bone metastasis.

References

1. Coleman RE: Bisphosphonates: clinical experience. Oncologist 9 (Suppl 4): 14-27, 2004.
2. Lipton A, Colombo-Berra A, Bukowski RM, Rosen L, Zheng M and Urbanowitz G: Skeletal complications in patients with bone metastases from renal cell carcinoma and therapeutic benefits of zoledronic acid. Clin Cancer Res 10: 6397S-6403S, 2004.
3. Destombe C, Botton E, Le Gal G, *et al*: Investigations for bone metastasis from an unknown primary. Joint Bone Spine 74: 85-89, 2007.
4. Iizuka Y, Iizuka H, Tsutsumi S, *et al*: Diagnosis of a previously unidentified primary site in patients with spinal metastasis: diagnostic usefulness of laboratory analysis, CT scanning and CT-guided biopsy. Eur Spine J 18: 1431-1435, 2009.
5. Katagiri H, Takahashi M, Inagaki J, Sugiura H, Ito S and Iwata H: Determining the site of the primary cancer in patients with skeletal metastasis of unknown origin: a retrospective study. Cancer 86: 533-537, 1999.
6. Kakhki VR, Anvari K, Sadeghi R, Mahmoudian AS and Torabian-Kakhki M: Pattern and distribution of bone metastases in common malignant tumors. Nucl Med Rev Cent East Eur 16: 66-69, 2013.
7. Bartels RH, van der Linden YM and van der Graaf WT: Spinal extradural metastasis: review of current treatment options. CA Cancer J Clin 58: 245-259, 2008.
8. Harel R and Angelov L: Spine metastases: current treatments and future directions. Eur J Cancer 46: 2696-2707, 2010.
9. Sutcliffe P, Connock M, Shyangdan D, Court R, Kandala NB and Clarke A: A systematic review of evidence on malignant spinal metastases: natural history and technologies for identifying patients at high risk of vertebral fracture and spinal cord compression. Health Technol Assess 17: 1-274, 2013.
10. Oken MM, Creech RH, Tormey DC, *et al*: Toxicity and response criteria of the Eastern Cooperative Oncology Group. Am J Clin Oncol 5: 649-655, 1982.
11. Katagiri H, Takahashi M, Wakai K, Sugiura H, Kataoka T and Nakanishi K: Prognostic factors and a scoring system for patients with skeletal metastasis. J Bone Joint Surg Br 87: 698-703, 2005.
12. Delank KS, Wendtner C, Eich HT and Eysel P: The treatment of spinal metastases. Dtsch Arztebl Int 108: 71-80, 2011.
13. Al-Brahim N, Ross C, Carter B and Chorneyko K: The value of postmortem examination in cases of metastasis of unknown origin - 20-year retrospective data from a tertiary care center. Ann Diagn Pathol 9: 77-80, 2005.
14. Blaszyk H, Hartmann A and Bjornsson J: Cancer of unknown primary: clinicopathologic correlations. APMIS 111: 1089-1094, 2003.
15. Rougraff BT, Kneisl JS and Simon MA: Skeletal metastases of unknown origin. A prospective study of a diagnostic strategy. J Bone Joint Surg Am 75: 1276-1281, 1993.
16. Han A, Xue J, Hu M, Zheng J and Wang X: Clinical value of ^{18}F-FDG PET-CT in detecting primary tumor for patients with carcinoma of unknown primary. Cancer Epidemiol 36: 470-475, 2012.
17. Ecker RD, Endo T, Wetjen NM and Krauss WE: Diagnosis and treatment of vertebral column metastases. Mayo Clin Proc 80: 1177-1186, 2005.
18. Sciubba DM, Petteys RJ, Dekutoski MB, *et al*: Diagnosis and management of metastatic spine disease. A review. J Neurosurg Spine 13: 94-108, 2010.

THE JOURNAL OF BIOLOGICAL CHEMISTRY VOL. 289, NO. 14, pp. 9865–9879, April 4, 2014

Human Immunodeficiency Virus Type 1 Enhancer-binding Protein 3 Is Essential for the Expression of Asparagine-linked Glycosylation 2 in the Regulation of Osteoblast and Chondrocyte Differentiation*[S]

Received for publication, September 20, 2013, and in revised form, January 26, 2014 Published, JBC Papers in Press, February 21, 2014, DOI 10.1074/jbc.M113.520585

Katsuyuki Imamura[‡§], Shingo Maeda[‡1], Ichiro Kawamura[§], Kanehiro Matsuyama[‡§], Naohiro Shinohara[‡§], Yuhei Yahiro[‡§], Satoshi Nagano[§], Takao Setoguchi[¶], Masahiro Yokouchi[§], Yasuhiro Ishidou[‡], and Setsuro Komiya[‡§¶]

From the Departments of [‡]Medical Joint Materials and [§]Orthopaedic Surgery and the [¶]Near-Future Locomotor Organ Medicine Creation Course, Graduate School of Medical and Dental Sciences, Kagoshima University, Kagoshima 890-8544, Japan

Background: The mechanisms by which Hivep3 regulates the osteochondrogenesis remain elusive.
Results: Knockdown of Hivep3 down-regulated *Alg2* expression. Alg2 suppressed osteoblast differentiation by inhibiting the activity of Runx2. Alg2 silencing suppressed the expression of *Creb3l2* and chondrogenesis.
Conclusion: Alg2 may be a modulator of osteochondrogenesis.
Significance: This is the first report to describe the association of an Alg gene with osteochondrogenesis.

Human immunodeficiency virus type 1 enhancer-binding protein 3 (*Hivep3*) suppresses osteoblast differentiation by inducing proteasomal degradation of the osteogenesis master regulator Runx2. In this study, we tested the possibility of cooperation of Hivep1, Hivep2, and Hivep3 in osteoblast and/or chondrocyte differentiation. Microarray analyses with ST-2 bone stroma cells demonstrated that expression of any known osteochondrogenesis-related genes was not commonly affected by the three Hivep siRNAs. Only *Hivep3* siRNA promoted osteoblast differentiation in ST-2 cells, whereas all three siRNAs cooperatively suppressed differentiation in ATDC5 chondrocytes. We further used microarray analysis to identify genes commonly down-regulated in both MC3T3-E1 osteoblasts and ST-2 cells upon knockdown of *Hivep3* and identified asparagine-linked glycosylation 2 (*Alg2*), which encodes a mannosyltransferase residing on the endoplasmic reticulum. The *Hivep3* siRNA-mediated promotion of osteoblast differentiation was negated by forced Alg2 expression. Alg2 suppressed osteoblast differentiation and bone formation in cultured calvarial bone. Alg2 was immunoprecipitated with Runx2, whereas the combined transfection of Runx2 and Alg2 interfered with Runx2 nuclear localization, which resulted in suppression of Runx2 activity. Chondrocyte differentiation was promoted by Hivep3 overexpression, in concert with increased expression of *Creb3l2*, whose gene product is the endoplasmic reticulum stress transducer crucial for chondrogenesis. *Alg2* silencing suppressed *Creb3l2* expression and chondrogenesis of ATDC5 cells, whereas infection of Alg2-expressing virus promoted chondrocyte maturation in cultured cartilage rudiments. Thus, Alg2, as a downstream mediator of Hivep3, suppresses osteogenesis, whereas it promotes chondrogenesis. To our knowledge, this study is the first to link a mannosyltransferase gene to osteochondrogenesis.

In skeletal development and bone remodeling, osteoblasts play major roles not only in bone formation but also in inducing the differentiation of bone-resorbing osteoclasts (1, 2). Runx2 is a critical transcription factor in osteoblast differentiation, as evidenced by Runx2 knock-out mice, which exhibit a complete lack of both intramembranous and endochondral ossification due to the absence of osteoblasts (3). Cleidocranial dysplasia, a human autosomal dominant inherited disorder of bone development, is characterized by hypoplasia of clavicles and abnormalities in cranial and facial bones and is caused by mutations in the *Runx2* gene (4, 5). Some genes, *e.g.* LDL receptor-related protein 5 (*Lrp5*), sclerostin (*Sost*), and human immunodeficiency virus type 1 enhancer-binding protein 3 (*Hivep3*), have been found to control osteoblast function in the adult human and/or mouse during postnatal skeletal remodeling (6–10).

Hivep3, also known as Schnurri-3, Zas3, and Krc, is a member of three mammalian homologs of the Hivep/Schnurri family of large zinc finger proteins. Hivep proteins have been studied for their roles in the regulation of an assortment of genes, including those encoding collagen type IIA, αA-crystallin, β-interferon, and HIV genes (11). Hivep2 can indirectly interact with the peroxisome proliferator-activated receptor γ2 (*Pparg2*) promoter to promote adipogenesis, through binding to Smad1, an intracellular mediator of bone morphogenetic protein (BMP)[2] signaling. Hivep2 can also dock to CCAAT/enhancer-binding protein α (C/ebpα) to interact

* This work was supported by Japan Society for the Promotion of Science KAKENHI Grants 23592221 (to S. M.) and 23592222 (to Y. I.), a grant from the Cell Science Research Foundation (to S. M.), and a grant from the Hip Joint Foundation of Japan (to S. M.).
[S] This article contains supplemental Tables 1–5.
[1] To whom correspondence should be addressed: Dept. of Medical Joint Materials, Graduate School of Medical and Dental Sciences, Kagoshima University, 8-35-1 Sakuragaoka, Kagoshima 890-8544, Japan. Tel.: 81-99-275-5381; Fax: 81-99-265-4699; E-mail: maeda-s@umin.ac.jp or s-maeda@m3.kufm.kagoshima-u.ac.jp.

[2] The abbreviations used are: BMP, bone morphogenetic protein; ER, endoplasmic reticulum; ALP, alkaline phosphatase; ECM, extracellular matrix; CDG, congenital disorders of glycosylation; qRT, quantitative RT; ALG, asparagine-linked glycosylation.

with a CCAAT site on the distal part of the *Pparg* gene (12). Mice lacking Hivep3 demonstrate adult-onset osteosclerosis with increased bone volume due to enhanced osteoblast activity (10). Hivep3 promotes proteasomal degradation of the Runx2 protein through recruitment of the E3 ubiquitin ligase Wwp1 to Runx2 (10). A D-domain motif within Hivep3 mediates the interaction with and inhibition of ERK mitogen-activated protein kinase (MAPK), thereby inhibiting Wnt/Lrp5 signaling through regulation of the activity of a downstream mediator glycogen synthase kinase 3-β (Gsk3β). This interaction results in the suppression of subsequent osteoblast differentiation (13). In addition, Hivep3 indirectly promotes osteoclastogenesis by promoting osteoblastic expression of receptor activator of nuclear factor-κB ligand (Rankl), a crucial factor for osteoclast differentiation (14). Hivep3 also cell-autonomously promotes osteoclastogenesis by inducing the expression of *Nfatc1*, a master transcription factor in osteoclast differentiation, by interacting with Traf6 to enhance its activity while forming a complex with c-Jun to activate the *Nfatc1* promoter (15). Thus, Hivep3 controls both bone formation and resorption at multiple steps to maintain normal bone mass. However, whether Hivep3 controls gene expression in osteoblasts to regulate osteoblast activity is unclear.

In contrast to *Hivep3* knock-out mice, mice lacking *Hivep2* exhibited decreased cortical bone volume and increased cancellous bone mass (16), suggesting different roles for Hivep2 and Hivep3 in the skeleton. Combined ablation of *Hivep2* and *Hivep3* in mice resulted in synergistically increased trabecular bone volume, demonstrating a redundancy between the two proteins in the regulation of postnatal bone mass (17). Interestingly, in the double knock-out mice, the growth plate cartilage of the long bones was uncoupled with bone phenotype, with significantly delayed maturation of chondrocytes resulting in chondrodysplasia (17), suggesting a role for Hivep proteins in the promotion of chondrocyte differentiation. However, the mechanism by which Hivep proteins affect chondrogenesis remains unknown. In addition, to date, no information has been reported on the possible role of Hivep1 in osteogenesis and/or chondrogenesis.

In this study, *in vitro* analysis showed that, among the three Hivep proteins, only Hivep3 was inhibitory and that the others promoted osteoblast differentiation. In contrast, all three Hivep genes seemed to support chondrocyte differentiation in BMP-2-induced ATDC5 cells, suggesting their redundancy in chondrogenesis. We found that asparagine-linked glycosylation 2 (*Alg2*) is commonly down-regulated in BMP-2-induced osteoblast differentiation in both MC3T3-E1 and ST-2 cells. Alg2 inhibited Runx2 activity without altering its protein level, resulting in suppression of osteoblast differentiation. Interestingly, in chondrogenesis of ATDC5 cells, Hivep3 induced the expression of cAMP-responsive element binding-protein 3-like 2 (*Creb3l2*), an endoplasmic reticulum (ER) stress transducer crucial for chondrogenesis (18), suggesting a possible role for Hivep3 in physiological mild ER stress. Alg2 was also decreased by *Hivep3* knockdown in ATDC5 chondrocytes, whereas silencing of Alg2 suppressed the expression of *Creb3l2* and chondrogenesis. To our knowledge, this study is the first to show a linkage between an asparagine-linked glycosylation mannosyltransferase gene and osteochondrogenesis.

EXPERIMENTAL PROCEDURES

Cell Culture and Differentiation—The mouse calvarial bone-derived osteoblast cell line, MC3T3-E1 (clone 4), and the mouse chondrogenic fibroblast cell line, C3H10T1/2, were obtained from the ATCC. The mouse bone marrow stromal cell line ST-2 and the mouse chondrogenic cell line ATDC5 were obtained from the RIKEN BioResource Center. MC3T3-E1 cells were cultured in minimum essential medium α (Invitrogen) containing 10% fetal bovine serum (FBS). ST-2 cells were cultured in RPMI 1640 medium (Sigma) containing 10% FBS. ATDC5 cells were cultured in Dulbecco's modified Eagle's medium (DMEM)/Ham's F-12 (1:1) (Invitrogen) containing 5% FBS. C3H10T1/2 cells were cultured in basal medium Eagle's (Sigma) with 2 mM L-glutamine and 10% FBS. COS-7 cells were purchased from RIKEN BioResource Center and maintained in DMEM supplemented with 10% FBS. All cell culture medium contained 100 units/ml penicillin G and 100 μg/ml streptomycin. Cell differentiation was induced by the addition of recombinant human BMP-2 (PeproTech) at a concentration of 300 ng/ml. Micromass culture of ATDC5 cells was performed as described previously (19) to accelerate the maturation of chondrocyte differentiation.

Alkaline Phosphatase (ALP) and Alcian Blue Staining—The activity of ALP secreted into the extracellular matrix (ECM) of cultured cells was visualized with an ALP staining kit (85L-3R, Sigma). Cartilaginous glycosaminoglycans produced in the ECM by cultured cells were stained with Alcian blue 8GX (Sigma).

RNA Interference—Dharmacon siRNA ON-TARGETplus SMARTpool, a mixture of four independent siRNAs against mouse *Hivep1*, *Hivep2*, *Hivep3*, and *Alg2*, and the control reagent were purchased from Thermo Scientific. siRNAs were transfected into cells using Lipofectamine RNAiMax (Invitrogen).

Real Time Quantitative PCR—Cells were lysed with TRIzol reagent (Invitrogen) to purify RNA, and 1 μg of total RNA was subjected to reverse transcription with the Verso cDNA kit (Thermo Scientific). The relative amounts of the gene transcripts were determined by real time quantitative PCR using SYBR premix Ex TaqII (Takara) and the Thermal Cycler Dice TP850 system (Takara). PCRs were performed in duplicate per sample, and the measured expression level of each gene was normalized to that of *Hprt1*. The sequence information for the primers used is listed in supplemental Table 1. All primer sets are for mouse genes, except for the m/h*Hivep3* primer set, which can be used to amplify both the mouse and human *Hivep3* genes. For evaluation of the tissue distribution of the Hivep genes and Alg2 *in vivo*, tissues were harvested from 3-month-old mice, and mRNA was purified with TRIzol reagent before subjecting samples to qRT-PCR.

Microarray Analysis—Cells transfected with siRNA overnight were further incubated with BMP-2 for 2 days before being lysed with TRIzol reagent for mRNA purification. mRNA samples were cleaned up using the RNeasy MinElute Cleanup kit (Qiagen) and analyzed on a Mouse Gene 2.0 ST Array (Affymetrix) by BioMatrix Research.

Plasmids, Adenovirus, and Lentivirus—The mouse Hivep3 expression plasmid, pEF-Shn3, was a kind gift from Dr. Laurie Glimcher (Harvard Medical School). The human HIVEP3 expression plasmid pFN21A-HIVEP3 was obtained from Kazusa DNA Research Institute. The mouse type II Runx2 expression plasmid was a kind gift from Dr. Toshihisa Komori (Nagasaki University). The FLAG-Runx2-def expression plasmid has been described in our previous study (20). Mouse *Alg2* or *Runx2* cDNA was cloned from ST-2 cells by using a RT-PCR-based technique, subcloned into the entry vector, pENTR, and further transferred into the C-terminally V5-tagged expression vector, pEF-DEST51 (Invitrogen). For overexpression assays, cells were transfected with expression vectors using FuGENE 6 (Roche Applied Science) or Lipofectamine 2000 (Invitrogen). Cells transiently expressing the transgenes were selected and enriched by incubation with G418 disulfate (Nacalai Tesque) at a concentration of 250 μg/ml for 3–7 days. To generate adenovirus-carrying *Alg2* cDNA, the *Alg2* gene in the pENTR-Alg2 vector was transferred into the C-terminally V5-tagged adenovirus expression vector pAd/CMV/V5-DEST by LR recombination (Invitrogen) and was further transfected into the adenovirus-producing cell line 293A according to the manufacturer's protocol. The pAd/CMV/V5-GW/lacZ adenovirus expression vector was used to generate a control adenovirus. For generation of lentivirus carrying the *Alg2* gene, pENTR-Alg2 and pENTR-5′EF1αP were subjected to LR recombination with pLenti6.4/R4R2/V5-DEST (Invitrogen) to generate a lentiviral vector expressing C-terminally V5-tagged Alg2 from the EF1α promoter. The lentiviral expression vector or pLenti6/V5/GW-lacZ control vector was transfected into 293FT cells to generate the lentivirus. Virus infection into ST-2 cells was performed at a multiplicity of infection of 100. Cells infected with the lentivirus were selected by treatment with blasticidin S HCl (Invitrogen) at a concentration of 2.5 μg/ml. These experiments were approved by the Kagoshima University safety control committee for gene recombination techniques (number 22053).

Embryonic Bone Organ Culture—Calvarial bone and metatarsal bone (cartilage) rudiments were harvested from C57BL/6J mouse embryos at 17.5 days post-coitum (E17.5) and cultured in minimum essential medium α or DMEM/Ham's F-12 (1:1), respectively, supplemented with 10% FBS, 100 units/ml penicillin G, and 100 μg/ml streptomycin, as described (21). The bone rudiments were incubated in virus solution overnight for infection of adenovirus or lentivirus. Cultured bones and cartilages were fixed in 96% ethanol and stained with 0.015% Alcian blue 8GX in a mixture solution of 96% ethanol/acetic acid (4:1) for 1 day, followed by a dehydration step in 100% ethanol. Dehydrated bones were immersed briefly in 1% potassium hydroxide (KOH), followed by staining in 0.001% alizarin red S (Sigma) in 1% KOH for 1 day. Images were captured with stereomicroscope M165FC (Leica). The animal experiments were approved by the Institutional Animal Care and Use Committee of Kagoshima University (number MD12137).

Immunoprecipitation and Immunoblotting—For immunoprecipitation assays, COS-7 cells were transfected with Alg2-V5 and/or FLAG-Runx2 plasmids and were lysed in M-PER lysis buffer (Thermo Scientific) supplemented with aprotinin and phenylmethylsulfonyl fluoride (PMSF). The lysate was immunoprecipitated with anti-FLAG M2-agarose affinity gel (A2220, Sigma), and the M2 antibody-bound protein complex was eluted by incubation with 3×FLAG peptide (F4799, Sigma), according to the manufacturer's protocol. For immunoblotting assays, cells were lysed in either M-PER or NE-PER lysis buffer (Thermo Scientific) supplemented with aprotinin and PMSF or directly with 1× SDS sample buffer. SDS-PAGE, membrane transfer, and chemiluminescence were performed using a standard protocol. The blots were incubated with primary antibodies against Alg2 (1:1000; LS-C81338, Lifespan Biosciences), Runx2 (1:200; M-70, sc-10758, Santa Cruz Biotechnology), Runx2 (1:1000; 8G5, MBL), Sp7 (1:1000, ab22552, Abcam), Ibsp (1:1000, LS-C190916, Lifespan Biosciences), type II collagen (1:1000, LS-C175971, Lifespan Biosciences), Creb3l2 (1:1000, ab76856, Abcam), V5 (1:5000; R960-25, Invitrogen), FLAG (1:1000; M2, F1804, Sigma), and tubulin (1:1000; DM1A, T9026, Sigma) and with horseradish peroxidase (HRP)-conjugated anti-rabbit and anti-mouse secondary antibodies (1:10,000) (Cell Signaling). For examination of half-life of Runx2 protein, after overnight transfection with siRNA of *Hivep3*, ST-2 cells were treated with cycloheximide (Sigma) at 100 μg/ml, followed by immunoblotting using anti-Runx2 antibody. Signals were detected using the LAS 4000 mini image analyzer (Fujifilm).

Immunofluorescence—For immunofluorescence assays, cells transfected with Runx2 and/or Alg2-V5 expression plasmids were fixed with 4% paraformaldehyde in PBS for 30 min and treated with 0.2% Triton X-100. CAS block (Zymed Laboratories Inc.) was used for blocking. Cells were incubated with anti-Runx2 (1:100; 8G5, MBL), Alexa Fluor 568 rabbit anti-mouse IgG (1:1000; A11061, Invitrogen), and anti-V5-FITC (1:500; R619-25, Invitrogen) antibodies. Nuclei were stained with Hoechst dye (Invitrogen). Confocal fluorescent imaging was performed and analyzed using a laser scanning microscope system (LSM 700, Zeiss). For confirmation of the efficiency of virus infection in cultured bones, formalin-fixed mouse E17.5 embryo calvariae or metatarsal bones were embedded in paraffin blocks, which were sliced at a 4-μm thickness. The antigen was retrieved by Liberate Antibody Binding (L.A.B.) solution (Polysciences). A CAS block was used for blocking. Bone sections were incubated with anti-V5-FITC antibody. Images were captured with microscope AX80 and digital camera DP70 (Olympus).

Luciferase Assay—COS-7 cells or ST-2 cells were seeded in triplicate in 24-well plates and transiently transfected with the 6×OSE2 luciferase reporter plasmid (a kind gift from Dr. Toshihisa Komori), the mutant 6×OSE2 luciferase reporter plasmid (a kind gift from Dr. Gerard Karsenty, Columbia University Medical Center), the pGL4.75hRlucCMV *Renilla* vector (Promega), and expression vectors for Runx2, Alg2, or Hivep3. Dual-Luciferase assays were performed as described earlier (20) by using the GloMax 96 microplate luminometer (Promega).

Statistical Analysis—The data in this study have been expressed as mean ± S.D. values of three independent experiments. Statistical comparisons between the different treatments were performed using an unpaired Student's *t* test in

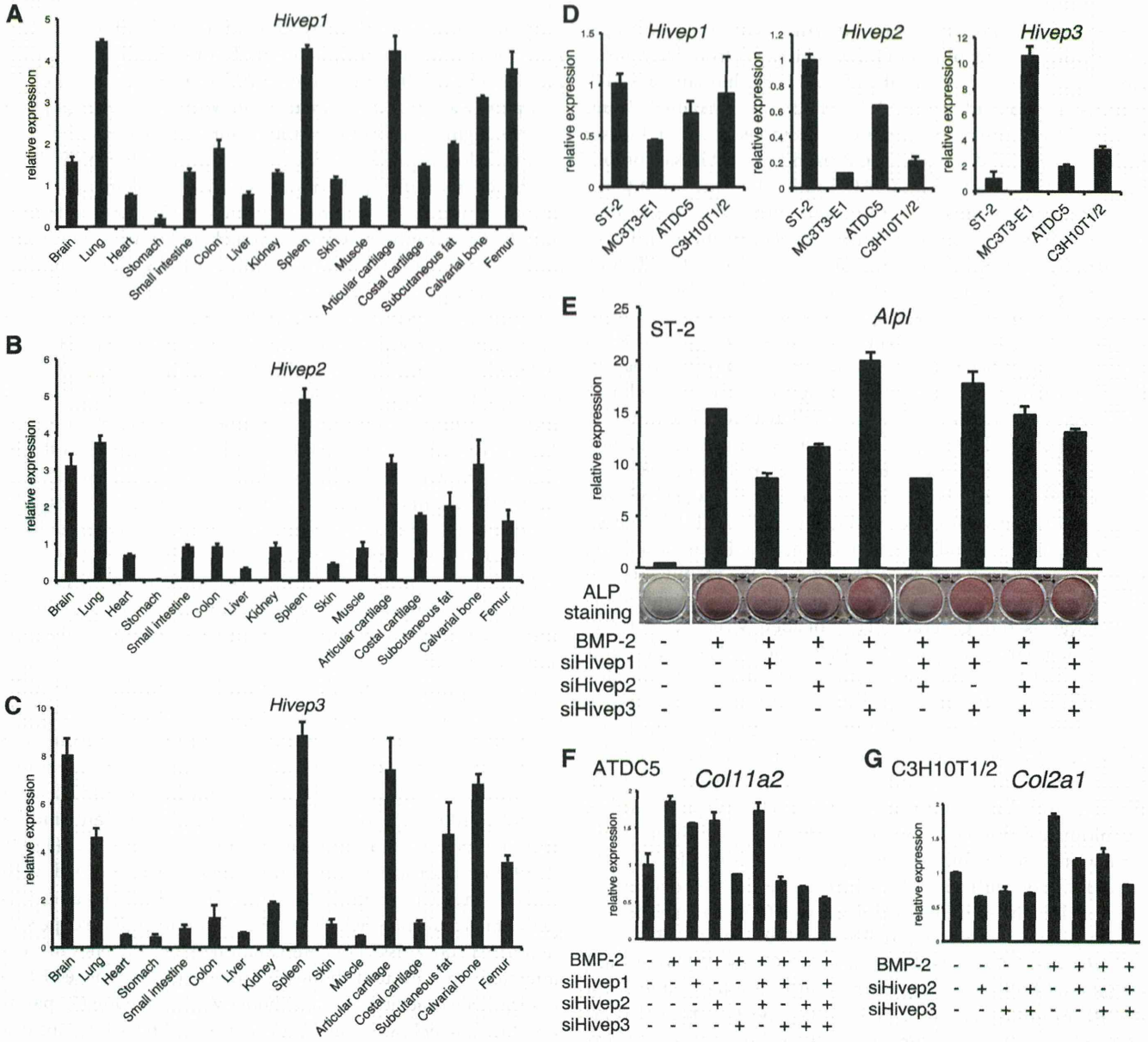

FIGURE 1. **All three Hivep genes are expressed in bone and cartilage to support osteochondrogenesis except Hivep3, which is inhibitory for osteoblast differentiation.** *A–C*, tissue cDNA panel of a 3-month-old mouse was subjected to quantitative RT-PCR (qRT-PCR) for *Hivep1* (*A*), *Hivep2* (*B*), or *Hivep3* (*C*). *D*, expression level of *Hivep1*, *Hivep2*, or *Hivep3* in the indicated cell lines was examined by qRT-PCR. *E*, ST-2 cells were transfected with siRNA for *Hivep1*, *Hivep2*, or *Hivep3* and treated with BMP-2 (300 ng/ml) for 6 days. Expression of *Alpl* was analyzed by qRT-PCR, and activity of ALP on ECM was visualized by ALP staining. *F*, ATDC5 cells were transfected with siRNA for *Hivep1*, *Hivep2*, and/or *Hivep3* and treated with BMP-2 (300 ng/ml) for 3 days. Expression of *Col11a2* was evaluated by qRT-PCR. *G*, C3H10T1/2 cells were transfected with siRNA for *Hivep2* and/or *Hivep3* and treated with BMP-2 (300 ng/ml) for 4 days. Expression of *Col2a1* was analyzed by qRT-PCR.

which $p < 0.05$ was considered significant, and $p < 0.01$ was considered highly significant.

RESULTS

Loss of Hivep1 or Hivep2 Suppresses Osteoblast Differentiation in ST-2 Cells, in Contrast to Hivep3 Silencing, and All Three Hivep siRNAs Inhibited Chondrogenesis—The precise roles of Hivep1 and Hivep2 in osteoblast differentiation are unclear. In a tissue cDNA panel from a 3-month-old adult mouse, all the Hivep genes showed a relatively specific expression pattern with high expression being observed in the lung, spleen, articular cartilage, and bone (Fig. 1, *A–C*). However, the *in vitro* results for the osteochondrogenic cell lines ST-2, MC3T3-E1, ATDC5, and C3H10T1/2 showed that the expression profiles were completely different between the Hivep genes, with *Hivep1* being expressed ubiquitously, *Hivep2* abundant in ST-2 and ATDC5, and *Hivep3* prominent in MC3T3-E1 osteoblasts (Fig. 1*D*). If the Hivep genes cooperate in osteoblast differentiation, they should regulate some common sets of genes. To test this hypothesis, ST-2 cells transfected with siRNA for *Hivep1*, *Hivep2, or Hivep3* were analyzed by a microarray assay (supplemental Tables 2–4, respectively), and the results were com-

TABLE 1

Genes down-regulated by loss of the Hivep family genes

ST-2 cells were transfected with siRNA for *Hivep1*, *Hivep2*, or *Hivep3* and treated with BMP-2 (300 ng/ml) for 2 days. mRNA samples were subjected to microarray analysis. *A*, expression of five genes was commonly decreased by all the siRNAs for the three Hivep genes. *B*, expression of six genes was commonly down-regulated by the *Hivep1* and *Hivep2* siRNAs. *C*, expression of four genes was commonly down-regulated by the *Hivep1* and *Hivep3* siRNAs. *D*, expression of three genes was commonly down-regulated by the *Hivep2* and *Hivep3* siRNAs.

A

Unique Sorted Transcript ClusterID	siCont	siHivep1	siHivep2	siHivep3	gene symbol	gene description
17305520	21.529846	11.831301	9.75173	7.9562707	*Ear1*	eosinophil-associated, ribonuclease A family, member 1
17467150	24.856544	14.449716	11.51435	15.580148	*Vmn1r18*	vomeronasal 1 receptor 18
17444697	31.70125	19.534565	21.051311	17.505947	*Cyp3a59*	cytochrome P450, subfamily 3A, polypeptide 59
17245120	44.998398	29.873207	26.863188	29.873207	*1700030O20Rik*	RIKEN cDNA 1700030O20 gene
17481207	17.905426	10.739602	10.739602	10.603919	*Olfr608*	olfactory receptor 608

B

Unique Sorted Transcript ClusterID	siCont	siHivep1	siHivep2	gene symbol	gene description
17278822	65.41499	39.391872	41.367386	*Mir679*	microRNA 679
17302598	42.895184	26.84824	22.885633	*Gm6280*	predicted gene 6280
17344852	19.322012	12.227982	11.5472975	*Olfr97*	olfactory receptor 97
17509018	24.977375	16.012548	11.412771	*Adam34*	a disintegrin and metallopeptidase domain 34
17495404	82.13324	52.76455	42.29805	*Rps13*	ribosomal protein S13
17541719	21.694231	14.250495	14.178923	*Mir450-2*	microRNA 450-2

C

Unique Sorted Transcript ClusterID	siCont	siHivep1	siHivep3	gene symbol	gene description
17356739	63.32018	36.357323	32.77719	*Mir194-2*	microRNA 194-2
17268088	22.22885	13.294091	13.626566	*Gm11543*	predicted gene 11543
17324996	19.940779	12.472511	12.472511	*Mir1947*	microRNA 1947
17516159	30.844234	20.207043	19.56977	*Olfr251|Olfr900*	olfactory receptor 251 I olfactory receptor 900

D

Unique Sorted Transcript ClusterID	siCont	siHivep2	siHivep3	gene symbol	gene description
17395379	248.2335	129.81422	142.53452	*LOC100504873*	zinc finger protein 14-like
17320035	82.69005	51.436905	49.273067	*Mir1249*	microRNA 1249
17366886	162.14816	104.84351	90.903786	*Mir467e*	microRNA 467e

pared. The expression of five genes decreased in all three knockdown experiments (Table 1, *A*), whereas six genes, four genes, or three genes were down-regulated in common by siHivep1 and siHivep2 (Table 1, *B*), siHivep1 and siHivep3 (Table 1, *C*), or siHivep2 and siHivep3 (Table 1, *D*), respectively, although no trend was observed in the purified genes. Moreover, none of the purified genes was reported to correlate with differentiation of osteoblasts or chondrocytes. To investigate the roles and possible synergism of the Hivep genes in osteoblast differentiation, the expression of the three Hivep genes was knocked down in ST-2 cells, alone or in combination (Fig. 1*E*). Although combined genetic ablation of the *Hivep2* and *Hivep3* genes in mice resulted in synergistically increased bone formation and bone volume (17), siRNA-mediated silencing of *Hivep2* in BMP-2-stimulated ST-2 cells decreased the expression and activity of ALP (Fig. 1*E*, compare *lanes 2* and *4*), whereas loss of *Hivep3* alone enhanced the osteoblast differentiation (Fig. 1*E*, compare *lanes 2* and *5*). Interestingly, combined transfection of siHivep2 with siHivep3 negated the enhancement of ALP production by *Hivep3* knockdown (Fig. 1*E*, compare *lanes 2, 5,* and *8*). Similar to siHivep2, *Hivep1* siRNA inhibited ALP activity; however, there was no synergistic or additive effect on combined knockdown of *Hivep1* and *Hivep2*. These results suggest that, in ST-2 bone marrow stromal cells, the cell autonomous actions of Hivep genes are diverse and show no cooperation in osteoblast differentiation and that Hivep1 and Hivep2 promote the counteraction of the suppressive effect of Hivep3. In contrast, in an siRNA-mediated knockdown assay in ATDC5 chondrocytes, siHivep1, siHivep2, and siHivep3 all decreased the BMP-2-induced expression of the chondrocyte-specific type XI collagen gene (*Col11a2*) (Fig. 1*F*). A similar result was observed in another chondrocytic cell line, C3H10T1/2, where knockdown of both *Hivep2* and *Hivep3* decreased the level of a chondrocyte marker, type II collagen gene (*Col2a1*) (Fig. 1*G*). In both experiments in chondrogenic cells, the combined loss of the Hivep genes showed some additive effects.

Hivep3 Suppresses Osteoblast Differentiation in Vitro—Although the mRNA level of Runx2 was comparable between wild-type and Hivep3 knock-out cells, the protein levels of Runx2, as well as the mRNA levels of the early osteoblast differentiation markers osterix (*Sp7*), alkaline phosphatase (*Alpl*), activating transcription factor 4 (*Atf4*), and bone sialoprotein (*Ibsp*) and of the late maturation marker osteocalcin (*Bglap2*) increased in knock-out osteoblasts (10). We first checked if this effect could be reproduced via siRNA-mediated knockdown in osteoblastic cell lines. We used the mouse bone marrow stromal cell line ST-2 as a model for premature osteoblast progenitors and MC3T3-E1 mouse calvaria-derived osteoblasts as mature osteoblasts. In both MC3T3-E1 and ST-2 cells, ~50% knockdown was achieved by transfection of siHivep3 (Fig. 2, *A* and *C*). As expected, *Hivep3* silencing did not have any effect on the mRNA expression of *Runx2* (Fig. 2, *A* and *C*). In ST-2 cells treated with cycloheximide to block *de novo* synthesis of Runx2

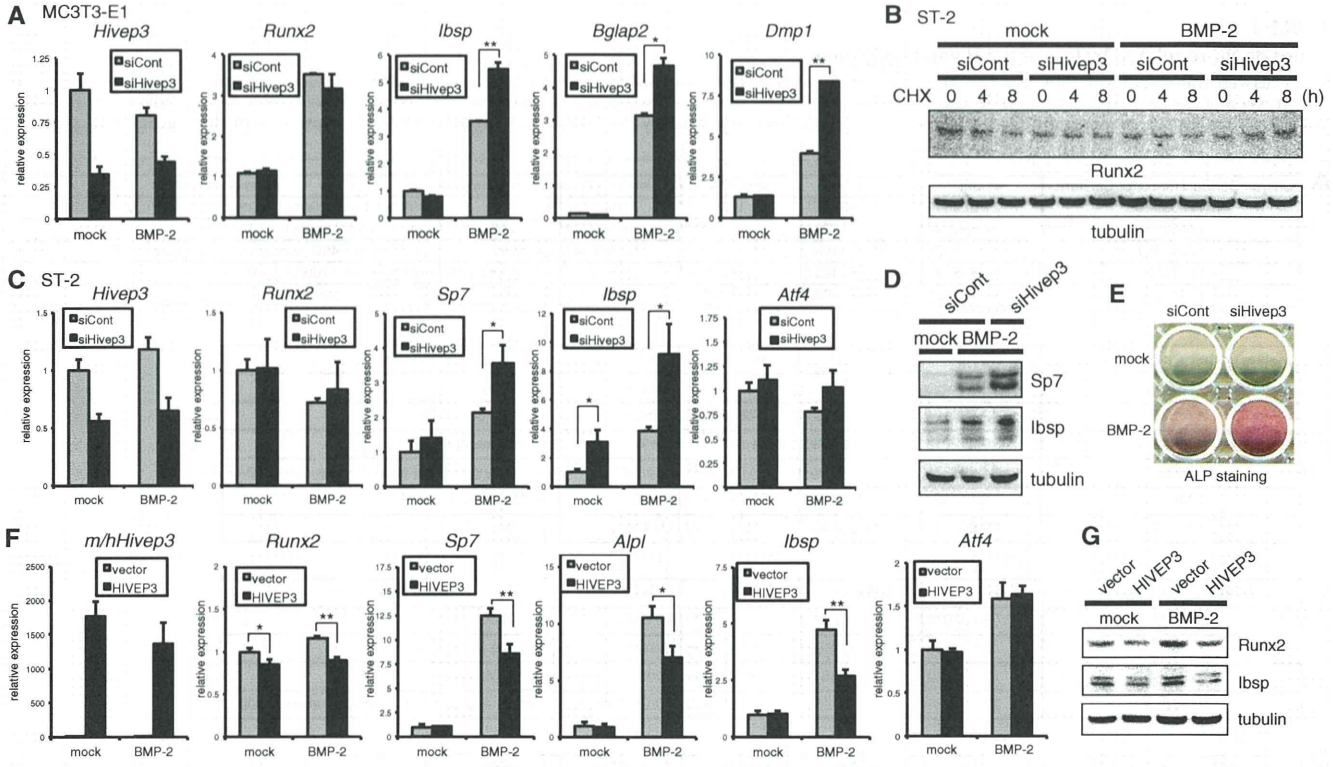

FIGURE 2. **Silencing of *Hivep3* increases protein stability of Runx2 to promote BMP-2-induced osteoblast differentiation.** *A*, MC3T3-E1 osteoblasts were transfected with siRNA for *Hivep3* with or without BMP-2 treatment (300 ng/ml) for 6 days. qRT-PCR analysis was performed for the indicated genes. *B*, siRNA-transfected ST-2 cells were treated with 100 μg/ml cycloheximide (*CHX*) with or without BMP-2 treatment (300 ng/ml) for the indicated time points. Cell lysates were analyzed by immunoblotting with an anti-Runx2 antibody. Tubulin served as a loading control. *C*, ST-2 cells were transfected with siRNA for *Hivep3* with or without BMP-2 treatment (300 ng/ml) for 3 days. The expression level of the indicated genes was examined by qRT-PCR. *D*, ST-2 cells were transfected with siRNA for *Hivep3* with BMP-2 treatment (300 ng/ml) for 7 days. Cell lysates were analyzed by immunoblotting with the indicated antibodies. Tubulin served as a loading control. *E*, ST-2 cells were transfected with *Hivep3* siRNA and stimulated with BMP-2 (300 ng/ml) for 6 days. ALP staining was performed. *F*, ST-2 cells were transfected with a human HIVEP3 expression vector and further stimulated with BMP-2 (300 ng/ml) for 4 days. The expression of the indicated genes was evaluated by qRT-PCR. *G*, ST-2 cells transfected with a human HIVEP3 expression vector were stimulated with BMP-2 (300 ng/ml) for 5 days. Cell lysates were analyzed by immunoblotting with the indicated antibodies. Tubulin served as a loading control. *, $p < 0.05$; **, $p < 0.01$.

protein, the protein level of Runx2 decreased in a time-dependent manner (Fig. 2*B*), although the protein expression was maintained in siHivep3-transfected cells. Moreover, combined induction of BMP-2 and siHivep3 in ST-2 cells increased Runx2 protein in a time-dependent fashion (Fig. 2*B*). Therefore, siRNA-mediated silencing of *Hivep3* stabilized Runx2 protein. As a result, expression of *Sp7*, *Ibsp*, and *Bglap2* was up-regulated in MC3T3-E1 and ST-2 cells (Fig. 2, *A* and *C*). In addition, the expression of an osteocyte marker, dentin matrix protein 1 (*Dmp1*), was elevated by *Hivep3* knockdown in MC3T3-E1 osteoblasts (Fig. 2*A*). The siHivep3-mediated increase of osteoblastic differentiation in ST-2 cells was confirmed by immunoblotting against Sp7 and Ibsp (Fig. 2*D*) or ALP staining (Fig. 2*E*). We introduced the human *HIVEP3* gene in ST-2 cells through transfection and confirmed the transgene expression by qRT-PCR (Fig. 2*F*). HIVEP3 suppressed BMP-2-induced osteoblast differentiation (Fig. 2, *F* and *G*) and protein expression of Runx2 (Fig. 2*G*). Interestingly, the mRNA expression of *Runx2* decreased following transfection with HIVEP3. As HIVEP3 destabilizes Runx2 protein, this result is likely due to loss of auto-induction of Runx2 (22), in which endogenous Runx2 mRNA expression increased in Runx2 transgenic mice (23). In both cases of knockdown and overexpression of *Hivep3*, expression of *Atf4* did not change (Fig. 2, *C* and *F*), although it increased in *Hivep3* knock-out osteoblasts (10).

Reduced Alg2 Gene Expression Following Knockdown of Hivep3—We next screened for genes whose expression was commonly reduced in both ST-2 cells and MC3T3-E1 cells upon *Hivep3* silencing by microarray analysis. The genes with decreased expression in MC3T3-E1 or ST-2 cells by >1.5-fold are listed in supplemental Table 5 (38 genes) or supplemental Table 4 (74 genes), respectively. Among these genes, only five were commonly down-regulated by siHivep3 in the two cell lines (Fig. 3*A*). For more stringent screening, we further increased the cutoff threshold to a >1.8-fold decrease, which left two genes each in the two cell lines, *Lypla2* and *Alg2* in MC3T3-E1 cells and *Alg2* and *Igfbp5* in ST-2 cells (Fig. 3*A*). Therefore, *Alg2* most commonly showed a decrease in expression due to *Hivep3* knockdown in both MC3T3-E1 and ST-2 cells. Asparagine-linked glycosylation (ALG) is one of the most common protein modification reactions in eukaryotic cells, as many proteins that are translocated across or integrated into the rough ER carry *N*-linked oligosaccharides (24). Alg2 is an α-1,3-mannosyltransferase forming a type I transmembrane protein on the ER, with its active site being cytosolically oriented (25). To date, no information has been reported to link

A

MC3T3-E1				
gene symbol	gene description	siCont	siHivep3	fold decrease
Lypla2	lysophospholipase 2	855.57886	385.55112	2.219106146
Alg2	**asparagine-linked glycosylation 2**	**1875.0286**	**875.0924**	**2.142663563**
Igfbp5	insulin-like growth factor binding protein 5	3540.0374	2207.5708	1.60358952
Ankfy1	ankyrin repeat and FYVE domain containing 1	1102.1857	719.4798	1.531920285
Gpr133	G protein-coupled receptor 133	545.9816	362.30106	1.50698317

ST-2				
gene symbol	gene description	siCont	siHivep3	fold decrease
Alg2	**asparagine-linked glycosylation 2**	**568.02734**	**314.0774**	**1.808558464**
Igfbp5	insulin-like growth factor binding protein 5	179.31311	99.23038	1.807038429
Lypla2	lysophospholipase 2	586.02966	349.82162	1.675224247
Ankfy1	ankyrin repeat and FYVE domain containing 1	1006.6627	650.5681	1.547359454
Gpr133	G protein-coupled receptor 133	93.81231	61.831158	1.517233593

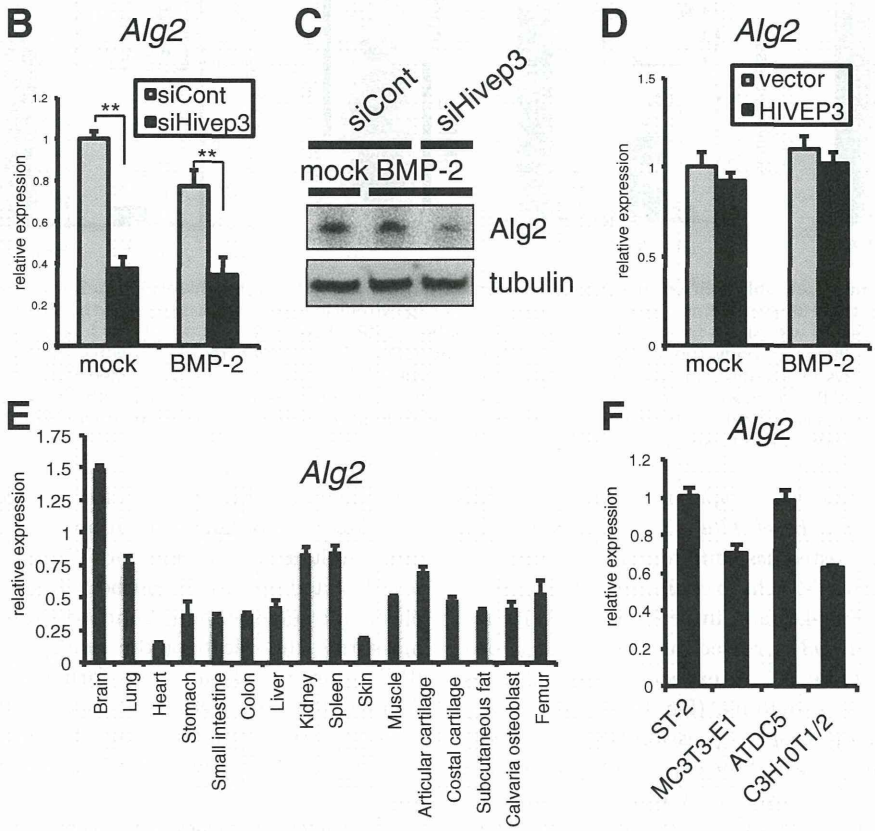

FIGURE 3. **Expression of the *Alg2* gene is reduced upon knockdown of *Hivep3* in osteoblastic cells.** *A*, siRNA for *Hivep3* was transfected into MC3T3-E1 or ST-2 cells prior to treatment with BMP-2 (300 ng/ml) for 2 days and analyzed by microarray. A list of five genes with decreased signal intensity, in common between MC3T3-E1 and ST-2 cells, is presented. *B*, ST-2 cells were transfected with siRNA for *Hivep3* with or without BMP-2 treatment (300 ng/ml) for 3 days. The expression level of *Alg2* was examined by qRT-PCR. *C*, ST-2 cells were transfected with siRNA for *Hivep3* with BMP-2 treatment (300 ng/ml) for 7 days. Cell lysates were analyzed by immunoblotting with an anti-Alg2 antibody. Tubulin served as a loading control. *D*, ST-2 cells were transfected with a human HIVEP3 expression vector to be stimulated with BMP-2 (300 ng/ml) for 4 days. The expression of *Alg2* was evaluated by qRT-PCR. *E*, tissue cDNA panel of a 3-month-old mouse was subjected to real time PCR for *Alg2*. *F*, expression level of *Alg2* in the indicated cell lines was examined by a qRT-PCR assay. **, $p < 0.01$.

Alg2 to cell differentiation. We confirmed the microarray results by qRT-PCR (Fig. 3*B*) or immunoblotting (Fig. 3*C*) and verified that knockdown of *Hivep3* in ST-2 cells decreased the level of *Alg2* by over 50%. However, forced expression of HIVEP3 did not increase *Alg2* expression (Fig. 3*D*). We next examined the tissue distribution of *Alg2* in 3-month-old mice by quantitative PCR analysis of a tissue cDNA panel (Fig. 3*E*). In tissues with low expression of *Hivep3* (Fig. 1*C*), *i.e.* the heart or skin, *Alg2* also showed a minimum level of expression, although both genes were highly expressed in the brain and lungs, suggesting a linkage between the levels of the two genes. However, there were some exceptions, *e.g. Hivep3* was expressed at high levels in fat, cartilage, and bone, whereas *Alg2* was detected at a moderate level in these tissues. From the osteoblastic and/or chondrocytic cell lines, MC3T3-E1 showed a significantly high level of *Hivep3* expression (Fig. 1*D*), whereas *Alg2* was detected in a relatively ubiquitous pattern (Fig. 3*F*). These results suggest that Hivep3 is essential but not sufficient for the expression of *Alg2*.

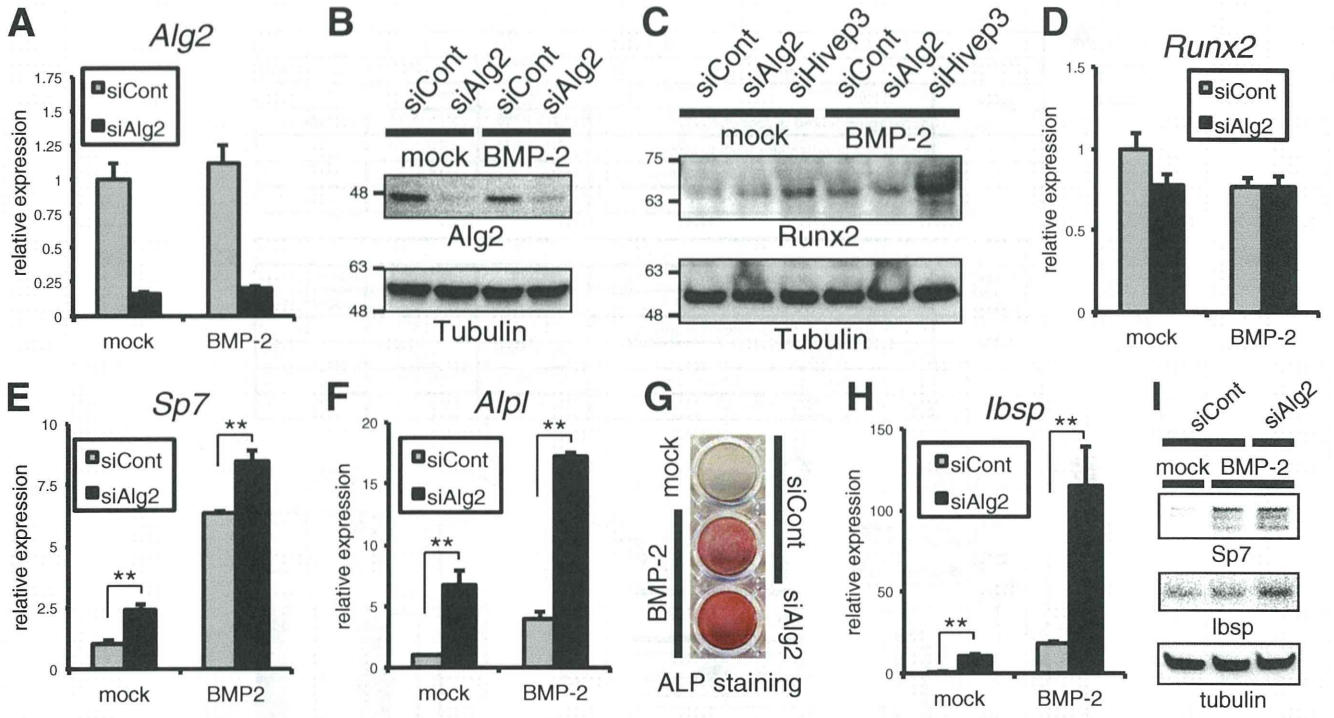

FIGURE 4. **Loss of Alg2 enhances osteoblast differentiation in ST-2 cells without affecting the protein level of Runx2.** *A* and *B*, ST-2 cells were transfected with siRNA for *Alg2* with or without BMP-2 treatment (300 ng/ml) for 3 days. Knockdown efficiency for *Alg2* was examined by qRT-PCR (*A*) or by immunoblotting (*B*). *C*, ST-2 cells were transfected with siRNA for *Alg2* or *Hivep3* with or without BMP-2 treatment (300 ng/ml) for 3 days. Cell lysates were analyzed by immunoblotting with an anti-Runx2 antibody. Tubulin served as a loading control. *D–F*, ST-2 cells were transfected with siRNA for *Alg2* with or without BMP-2 treatment (300 ng/ml) for 3 days. Expression of indicated genes was analyzed by qRT-PCR. *G*, ST-2 cells were transfected with siRNA for *Alg2* and treated with BMP-2 (300 ng/ml) for 6 days. ALP staining was performed. *H*, ST-2 cells were transfected with siRNA for *Alg2* with or without BMP-2 treatment (300 ng/ml) for 3 days. Expression of *Ibsp* was analyzed by qRT-PCR. *I*, ST-2 cells were transfected with siRNA for *Alg2* with BMP-2 treatment (300 ng/ml) for 2 days. Cell lysates were analyzed by immunoblotting with indicated antibodies. **, $p < 0.01$.

Loss of Alg2 Promotes Osteoblast Differentiation in ST-2 Cells without Affecting the Protein Level of Runx2—To investigate the possible role of Alg2 in osteoblast differentiation, siRNA for *Alg2* was transfected into ST-2 cells to obtain an ~80% decrease in mRNA expression (Fig. 4*A*) and in protein level (Fig. 4*B*). Although silencing of *Hivep3* increased the level of Runx2 protein, siAlg2 had no effect (Fig. 4*C*). As expected, loss of Alg2 also did not change the RNA level of Runx2 (Fig. 4*D*). However, *Alg2* knockdown mildly enhanced *Sp7* expression (Fig. 4, *E* and *I*), although it dramatically increased the expression (Fig. 4*F*) and activity (Fig. 4*G*) of ALP. A similar effect was seen on the level of *Ibsp* mRNA (Fig. 4*H*) and protein (Fig. 4*I*), suggesting a suppressive role of Alg2 in osteoblast maturation.

Forced Expression of Alg2 Inhibits Osteoblast Differentiation and Bone Formation—We investigated the effect of overexpression of Alg2 in osteoblasts by infection of adenovirus or lentivirus carrying an Alg2 expression cassette. In ST-2 cells, forced expression of Alg2 showed no effect on Runx2 protein level (Fig. 5*A*), whereas it strongly suppressed the expression of *Sp7*, *Alpl*, and *Ibsp* (Fig. 5*B*). The lentivirus-mediated expression of the Alg2 transgene product was confirmed at the protein and mRNA level (Fig. 5, *C* and *D*). Combined induction of *Hivep3* siRNA with the Alg2 lentivirus completely negated the enhanced expression of *Ibsp* by siHivep3, suggesting that Alg2 is a downstream mediator of Hivep3 for blocking osteoblast differentiation (Fig. 5*E*). To assess the role of Alg2 in osteoblastic bone formation, we employed the *ex vivo* culture system of calvarial bone harvested from E17.5 mouse embryo. The infection efficiency of lentivirus in bone culture was evaluated by immunofluorescence, and the V5-tagged transgene product was detected by anti-V5 antibody (Fig. 5*F*). The rate of osteoblastic intramembranous bone formation can be examined by measuring the width of the fontanelle (20). Application of BMP-2 promoted the bone formation, and it significantly decreased the fontanelle width, whereas combined induction of Alg2-expressing lentivirus cancelled the narrowing (Fig. 5*G*), indicating that Alg2 inhibited BMP-induced osteoblastic bone formation.

Alg2 Knockdown Does Not Affect ER Stress nor BMP Signaling in ST-2 Cells—A defect in ALG may affect the quality control of protein folding in the ER, which might subsequently evoke ER stress (26, 27). In addition, because physiologically mild ER stress is required for proper osteoblast differentiation and maturation (28, 29), we investigated the effect of *Alg2* siRNA on ER stress-related genes by qRT-PCR (Fig. 6*A*). Atf4, a downstream target of PKR-like endoplasmic reticulum kinase of ER stress transducer, is crucial for the expression of *Bglap2* and synthesis of type I collagen during osteoblast maturation (28, 30). *Alg2* silencing showed no remarkable effect on the *Atf4* mRNA level (Fig. 6*A*). An ER stress transducer called cAMP-responsive element-binding protein 3-like 1 (*Creb3l1*), alternatively known as Oasis, is also crucial in osteoblast differentiation (29). However, the level of *Creb3l1* was unchanged by Alg2 silencing (Fig. 6*A*). DNA damage-inducible transcript 3 (*Ddit3*), a target gene of